3B2v8.06a/w (Dec 5 2003).51c
XML:ver:5.0.1 DSRI : 1207 Prod.Type:COM
pp.1–18(col.fig.:4,6,7,11) ED:Sushma
PAGN:Dini SCAN:Dominic

Available online at www.sciencedirect.com

SCIENCE @ DIRECT®

Deep-Sea Research I ▮ (▮▮▮▮) ▮▮▮–▮▮▮

DEEP-SEA RESEARCH
PART I

www.elsevier.com/locate/dsr

The West Spitsbergen Current volume and heat transport from synoptic observations in summer

Waldemar Walczowski*, Jan Piechura, Robert Osinski, Piotr Wieczorek

Institute of Oceanology, Polish Academy of Sciences, Powstancow Warszawy 55, 81-712 Sopot, Poland

Received 28 June 2004; received in revised form 6 December 2004; accepted 15 March 2005

Abstract

This study describes the results of quasi-synoptic hydrographic observations of the West Spitsbergen Current made in summer 2003. Various sources of information and calculation methods were used to estimate the northward volume and heat transport. Ultimately, the results based on the Lowered Acoustic Doppler Current Profiled data were selected as the most reliable. The results of direct current measurements in the entire water column with relatively high horizontal resolution confirm the complicated, multi-path structure and high barotropic component of the West Spitsbergen Current. Measurements show high temporal variability of the volume transport and strong current dependence on wind conditions. The quasi-synoptic northward volume transport across section 78°50′N from 002°E to the Spitsbergen shelf is estimated at 11.6 Sv, and total heat transport at 70.6 TW.

Keywords: Arctic; Nordic seas; Circulation; West Spitsbergen Current; Atlantic water masses; Horizontal advection

1. Introduction

The Fram Strait is a passage between Greenland and Spitsbergen and is the only deep strait connecting the Nordic Seas and the Arctic Ocean (AO). The West Spitsbergen Current (WSC) carries warm, salty Atlantic Water (AW) northward and provides a large amount of heat and salt to the AO via the strait.

Investigations of the AW inflow into the AO have been the focus of many national and international research projects launched in recent years. In the context of observed climate change, the estimate of volume and heat carried northward by AW is an important task. AO warming, changes in its thermohaline structure, and significant sea ice retreat is related to the increased AW inflow into the AO (Zhang et al., 1998; Dickson et al., 2000; Karcher et al., 2003). Schauer et al. (2004) explained the warming events of the

*Corresponding author. Tel.: +48 58 551 72 81; fax: +48 58 551 21 30.

E-mail addresses: walczows@iopan.gda.pl (W. Walczowski), Roberto@iopan.gda.pl (R. Osinski).

0967-0637/$ - see front matter
doi:10.1016/j.dsr.2005.03.009

AO observed until 2000 by the increase of both the inflowing water temperature and flow strength.

The Nordic (Norwegian, Greenland, and Iceland) Seas play a crucial role in the distribution of warm, salty water carried northward by the Meridional Overturning Cell. Most of the AW enters the Nordic Seas over the Faroe-Iceland Ridge and between the Faroe and Shetland Islands (Hansen and Østerhus, 2000). The colder, less saline western branch of the Norwegian Atlantic Current is topographically guided from the Iceland-Faroe Front toward Fram Strait. In the Nordic Seas it appears as the jet of the Polar Front (Orvik and Niiler, 2002). The Polar Front, also called the Arctic Front (Swift, 1986), the Polar Ocean Front (Johannessen, 1986) or the Arctic Frontal Zone (van Aken et al., 1995), is the transition zone that divides Arctic and Atlantic waters and limits the western range of AW in the Nordic Seas. In the Greenland Sea, the front follows the Mohns and Knipovich ridges. The name used in this paper is the Arctic Front (AF).

The warmer, more saline eastern branch of AW inflows through the Faroe-Shetland Channel and continues north along the Norwegian shelf edge as the Norwegian Atlantic Slope Current (Orvik and Skagseth, 2003). After passing the Lofoten Islands, the current bifurcates. One stream of AW enters the Barents Sea as the North Cape Current and after undergoing significant modification, flows into the AO, mostly through the St. Anna Trough (Schauer et al., 2002; Maslowski et al., 2004). The second branch continues north as the WSC (Aagaard and Carmack, 1989).

It is well known that the main flow of the WSC is topographically guided and flows along the Barents Sea continental slope with streamlines of f/H (Coriolis parameter/column depth) (Hopkins, 1991). The complicated topography of the Fram Strait causes the WSC to split into three branches (Quadfasel et al., 1987). Only a fraction of AW enters and remains in the AO, while the majority recirculates and then flows south with the East Greenland Current (EGC) as the Return Atlantic Current (RAC) (Perkin and Lewis, 1984; Quadfasel et al., 1987; Rudels, 1987; Bourke et al., 1988). The Svalbard branch (Aagaard et al., 1987; Saloranta and Haugan, 2001) follows the Spitsbergen slope, crosses the Yermak Plateau and reaches the AO. The second branch follows the western rim of the Yermak Plateau and mixes with ambient waters by tidal mixing (Gascard et al., 1995), while the third one recirculates between 78° and 80°N. It is estimated that from 50% (Rudels, 1987) to 67% (Manley, 1995) of the northward flowing AW recirculates into the EGC by different pathways. The ratio of recirculation varies over time (Rudels et al., 2000).

It is less well known that the WSC has a multipath structure before reaching the south Spitsbergen latitude. Investigations conducted by the Institute of Oceanology (IOPAS) (Piechura and Walczowski, 1995) show that apart from the main flow of AW along the Barents Sea shelf break, a second weaker flow that carries AW northward is correlated with the Arctic Front. Due to bottom topography, both flows converge in the west region of Spitsbergen.

Estimates of volume transport by the WSC depend on the method applied. In general, direct measurements produce much higher results than indirect calculations. Using current meter data from the 1971–1972 period, Aagaard et al. (1973) reported the mean transport at 79°N to be 8 Sv. For the 1976–1977 period at 79°N, Hanzlick (1983) estimated a mean transport of 5.6 Sv with strong seasonal variability (from 1.4 Sv in March to 11.9 Sv in December). At the same latitude in the 1997–1999 period, Fahrbach et al. (2001) reported 9.5 Sv as the mean WSC transport. Their measurements show a significant maximum in spring (March) and the minimum in summer (August). The annual mean northward transport recorded over three years of measurements (1997–2000) indicates values between 9 and 10 Sv (Schauer et al., 2004). Transport estimates from hydrographic data are much lower. Baroclinic methods produce 2–3 Sv during the summer period (Piechura et al., 2001). Geostrophic transport for the same period that was referenced with the vessel-mounted Acoustic Doppler Current Profiler (VM-ADCP) data was 6–9 Sv (Osinski et al., 2003). Using a similar method, Cisewski et al. (2003) obtained northward transport of 11.5 Sv for a section along 79°40′N in September 1997.

Inverse methods applied by Rudels (1987), Schlichtholz and Houssais (1999) produced transports of 3.0 and 1.1 Sv, respectively. The large differences between the measured transports and those computed from hydrological data indicate that the barotropic (depth-independent) component of the WSC flow is significant.

Modeling efforts produce medium values. Karcher et al. (2003) pointed out that modeled volume flux into AO via the Fram Strait fluctuates between 2 and 3 Sv interannually. Using a 9-km resolution model, Maslowski et al. (2004) reported 6.4 Sv as the mean northward transport via the Fram Strait.

More detailed reviews of transport estimates were published by Hopkins (1991) and Simonsen and Haugan (1996).

This paper concentrates on the northern part of the Atlantic Domain, north of the 75°N parallel. Results of quasi-synoptic measurements conducted in the WSC during summer 2003 are presented. The questions the present authors sought to answer included the following: What are the main pathways of AW? What was the volume transport of AW across selected sections? Which mechanisms caused short-term transport variability?

Various methods of volume transport calculation were used. The indirect method—baroclinic calculations from the hydrographic data, was compared with direct measurements performed using VM-ADCP and LADCP. The mixed method, in which VM-ADCP data and baroclinic calculations are both used was also applied. The results of transport calculations depend strongly on the method applied. Calculations based on in situ observations produce the highest transport values.

2. Data and methods

Hydrographic observations along several sections in the Atlantic Domain of the Norwegian/Greenland Seas were carried out in June and July 2003 during an R.V. *Oceania* cruise. This was the Polish contribution to the Arctic-Subarctic Oceanic Flux Array for European climate: North (ASOF-N) FP5 project. Currents were recorded continuously with a 150 kHz VM-ADCP on the transects. The records extended down to about 400 m and were averaged every 5 min, which resulted in approximately 0.75 km spatial resolution at a vessel speed of five knots. The vertical resolution was set to 8 m. GPS navigation was applied as a reference during the measurements. The bottom reference was applied over the shelf.

A Seabird 9/11 CTD system was employed to conduct hydrographic observations. Sensors were calibrated by the Seabird service and water samples were taken. CTD casts were conducted from the surface to the bottom. Fig. 1 shows the CTD/LADCP grid of stations studied during the summer 2003 cruise in the WSC region. The position of sections ‘K’, ‘N’, ‘S’, ‘Z’, and ‘EB’, as well as wind conditions, during the measurements are presented in Table 1. The time necessary to perform one section was 2–3 days, so hydrological fields and transport calculations can be regarded as synoptic snapshots.

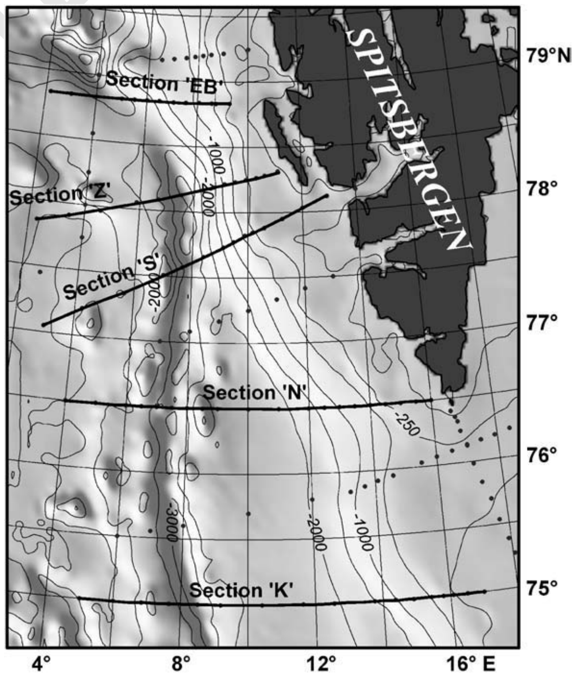

Fig. 1. Grid of stations studied during the summer 2003 cruise in the WSC region. The names of sections are indicated.

Table 1
Location of investigated sections and wind conditions during measurements

Section	Latitude (N)	Longitude (E)	Date	Wind direction	Wind speed ($m\,s^{-1}$)
K	75°00′	005°00′–017°00′	July 03–05	N–E	Decreasing 10–4
N	76°30′	004°00′–016°00′	July 05–07	NE	2–3
S	77°03′–78°05′	003°00′–012°55′	July 11–12	NE–E	Increasing 3–6
Z	77°51′–78°19′	002°18′–011°07′	July 13–14	SE	9–11
EB	78°50′	002°11′–009°16′	July 14–15	S–SW	7–11

The CTD data were processed with Seabird software; ultimately, vertical profiles of potential temperature, salinity, potential density, and specific volume anomaly (δ), averaged every 5 dbar, were calculated. To obtain vertical sections and horizontal distributions of properties, objective analysis methods were applied (Bretherton et al., 1976). Spatially non-uniform data were estimated into rectangular grids with kriging techniques (Emery and Thomson, 2001). The size of the vertical grid cell was $5\,m \times 2.5\,km$, while horizontal grid cells were $\sim 12 \times 12\,km$. To consider the different horizontal and vertical scales, the anisotropy ratio was applied for vertical sections. This technique determined the corelation between measured and estimated values higher than 0.9.

The baroclinic currents were computed in reference to the 1000 dbar layer of no motion (LNM). The vertical integration of the gridded fields of specific volume anomaly was applied for computing the geopotential anomaly (Φ') distributions at isobaric surfaces. In regions shallower than 1000 dbar, prior to integration the data gaps between LNM and bottom were filled in by the nearest values of δ measured at the same level. This allowed obtaining null near-bottom velocities and a realistic distribution of the Φ' field. Velocity components were derived from the horizontal gradients of geopotential anomaly considering the balance between the Coriolis force and the pressure gradient.

To reduce the effect of mesoscale activity and uneven cross-track and along-track data spacing, the grid of temperature utilized in Fig. 3 and geopotential anomaly used for calculations of geostrophic current presented in Fig. 8 were smoothed and filtered with a linear convolution low-pass filter. Therefore, these distributions rather show general patterns than synoptic pictures. The mean residual for the Φ' field is $1.3 \times 10^{-2}\,J\,kg^{-1}$ (with standard deviation of $14.4 \times 10^{-2}\,J\,kg^{-1}$). The currents presented in Fig. 5 were derived from a non-smoothed geopotential anomaly field and reveal a quasi-synoptic picture. In this case, the mean residual for the Φ' field was $0.1 \times 10^{-2}\,J\,kg^{-1}$, with standard deviation of $4.0 \times 10^{-2}\,J\,kg^{-1}$ and a correlation between measured and estimated values of 0.92.

Additionally, a self-recording Work Horse Sentinel ADCP 300 kHz device (LADCP) was lowered along with the CTD probe. The mean vertical profiling speed was $1\,m\,s^{-1}$. Measurements from down and up casts were averaged vertically in 20-m-thick boxes. Navigational data from the GPS were collected in CTD files. Fischer and Visbeck (1993) developed techniques for LADCP data processing. The data collected were processed using LDEO version 7.0 software (http://www.ldeo.columbia.edu/~visbeck/ladcp/) developed by Visbeck and Krahmann. Current profiles were corrected for tidal motions by subtracting the vertically homogenous tide component. For every LADCP cast, K1, O1, M2, and S2 tidal components were calculated using amplitudes and phases of tidal velocity components U and V given by Kowalik (1994) and Kowalik and Proshutinsky (1995). The tidal data are available via anonymous ftp: ftp.ims.uaf.edu. Vertical velocity profiles were gridded into sections and the same methods were applied as with the CTD profiles.

The method described by Cokelet et al. (1996) and Meinen et al. (2000) was used to calculate absolutely referenced geostrophic currents. Velocities measured by VM-ADCP were averaged spatially between CTD stations and vertically in the 50–150 m layer. Choosing this layer permits eliminating primarily wind-driven ageostrophic flows.

3. Hydrography

Traditionally, the salinity of AW entering the Nordic Seas has been described as $S>35$, and the potential temperature as $\theta>3\,^{\circ}\mathrm{C}$. In fact, the temperature and salinity of inflowing AW are higher and depend on how the water was transported (Hansen and Østerhus, 2000). The properties of the AW change significantly as it flows northward. The primary factors that modify AW temperature and salinity are mixing with fresher and colder ambient water and heat loss to the atmosphere (Piechura et al., 2002).

The downstream modification of AW thermohaline properties means that water masses in the northern part of the Greenland Sea are difficult to define. Apart from 'pure' AW, other water masses of Atlantic origin have been identified, such as the Returned AW (RAW), the modified AW, the Intermediate AW, etc. Schlichtholz and Houssais (1999) identified four water masses of AW origin in the Fram Strait region (AW warm, fresh, cold, and modified). Friedrich et al. (1995) proposed classifying AW based on water density.

Since the focus of this paper is volume and heat transport in the north-eastern part of the Atlantic Domain, there is no need to define AW precisely. Here AW is defined as water with a salinity of $S>34.92$ and a temperature of $\theta>0\,^{\circ}\mathrm{C}$ (Fig. 2). This parameterization is close to that of the water defined by Schlichtholz and Houssais (1999) as AW warm ($S>34.91$, $\theta>2\,^{\circ}\mathrm{C}$) and AW cold ($S>34.91$, $0\,^{\circ}\mathrm{C}<\theta<2\,^{\circ}\mathrm{C}$). It is also similar to water masses described by Swift and Aagaard (1981) as AW ($S>34.90$, $\theta>3\,^{\circ}\mathrm{C}$) and RAW ($S>34.90$, $\theta>0\,^{\circ}\mathrm{C}$). Salt, freshwater, and heat transported by AW are calculated in reference to $S=34.92$ and $\theta=0\,^{\circ}\mathrm{C}$. In order to make comparisons with other results, calculations based on the Swift and Aagaard (1981) AW classification ($S>34.9$, $\theta>3\,^{\circ}\mathrm{C}$) are also presented in the final results. The heat transported in the entire water

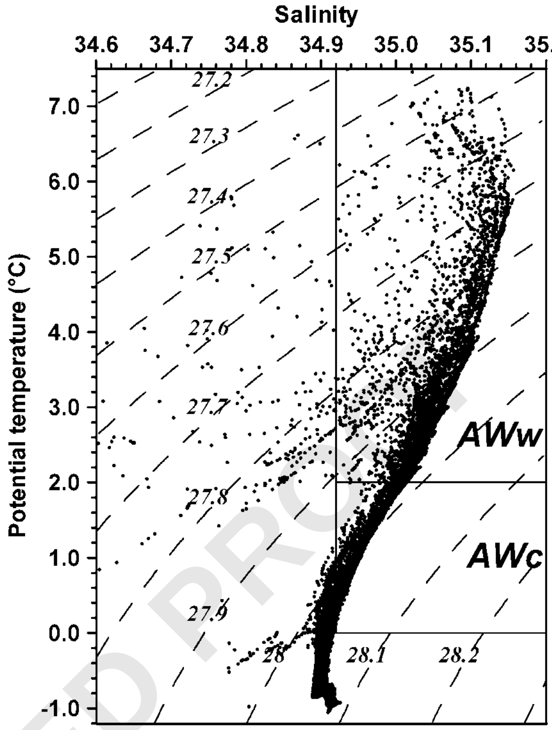

Fig. 2. TS diagram for water masses observed in the sampling area; AWw—Atlantic Water warm, AWc—Atlantic Water cold.

column is calculated in reference to a temperature of $-0.1\,^{\circ}\mathrm{C}$.

The horizontal temperature distribution at 100 dbar (Fig. 3) indicates that there are two convergent zones of high horizontal temperature gradients. The main warm flow of AW is situated over the Spitsbergen slope, while the second is located along the Mohns and Knipovich underwater ridges system. The shape of the isotherms in the western branch suggests AF bifurcation and intensive westward AW recirculation.

The AW layer in the central part of the section along the 76°30′N parallel (Fig. 4) is as thick as 750 m. AW occupies 155 km^2, which is 28% of the total area of the section. The core of AW is located over the continental slope, approximately along the 1000 m isobath. In this region, AW reaches a maximum salinity of 35.14 and a temperature of 6.9 °C. Strong baroclinicity occurred over the slope and the shape of the isopycnal surfaces suggested

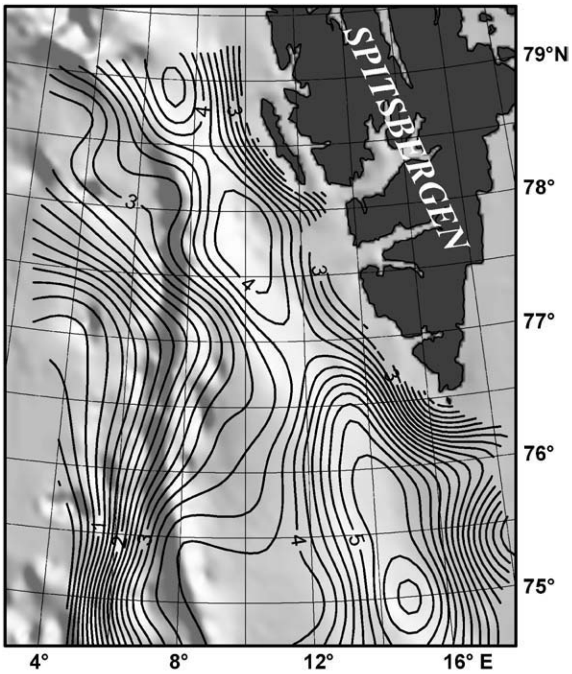

Fig. 3. Low-pass filtered horizontal temperature distribution at 100 dbar.

bi-directional baroclinic flow—northward over the deeper part of the slope and southward close to the shelf break. The second zone of high baroclinicity occurred in the region of the AF. The front usually divides Arctic and Atlantic water masses, but in this region AW occurred even west of the front. This water is colder and fresher (AWc) and occupies the upper 250 m layer to the west of the Knipovich Ridge.

4. Currents and transports

4.1. Baroclinic flows

The WSC has a strong barotropic component (Fahrbach et al., 2001; Schauer et al., 2004). The depth-independent part of the flow is much higher than the flow generated by the horizontal density gradients. However, in the case of AW transport, the baroclinic and barotropic components are comparable. As was previously stated, although baroclinic calculations underestimate current velocities and transport, they are still very useful. Baroclinic flow is more stable than the barotropic one; therefore, the hydrography-based method helps in the study of selected water mass pathways and the analysis of historical data, etc.

Vectors of baroclinic currents at 100 dbar computed from hydrographic data (Fig. 5) show zones of intensive northward flow in the southern part of the investigated area. Regions of slow movement and recirculation exist between them. The convergence of northward flows is steered by bottom topography and occurs at 77°N. Intense mesoscale activity and westward recirculation appear north of the 77°N parallel.

Fig. 6 presents the velocities across section 'N' that were calculated in reference to 1000 dbar. The positive value indicates the northward flow. Velocity distribution confirms the horizontal pattern of currents presented in Fig. 5. A zone of slow motion and recirculation separates the regions of northward flow over the slope and over the Knipovich Ridge. There is an intense southward counter-current east of the 13°30′E meridian. The horizontal current distribution also shows south and south-eastern flows between Sørkapp (the southern tip of Spitsbergen) and Bear Island; computed net volume transport at cross-section 'N' is 1.9 Sv at 3.6 Sv of northward and 1.7 Sv of southward transport. The net, northward, and southward transports of AW are estimated at 1.5, 2.9, and 1.4 Sv, respectively (Table 2). At this transect AW carries northward 18.9 TW of heat (1 TW$\equiv10^{12}$ W). Currents at the same section, calculated in reference to the bottom are presented in Fig. 9a.

While the baroclinic transport across sections 'N', 'S', and 'Z' are very similar, those across external sections differ significantly from the mean value. Section 'K' is opened to the east, and eastward transport between sections 'K' and 'N' (Fig. 5) might explain the decrease of transport across section 'N' against section 'K'. Sections 'N', 'S', 'Z', and 'EB' are closed in the east by the Spitsbergen shelf. Northward transport differences result mainly from the westward recirculation that occurs between sections. Table 2 suggests that recirculation between sections 'S' and 'Z' is limited

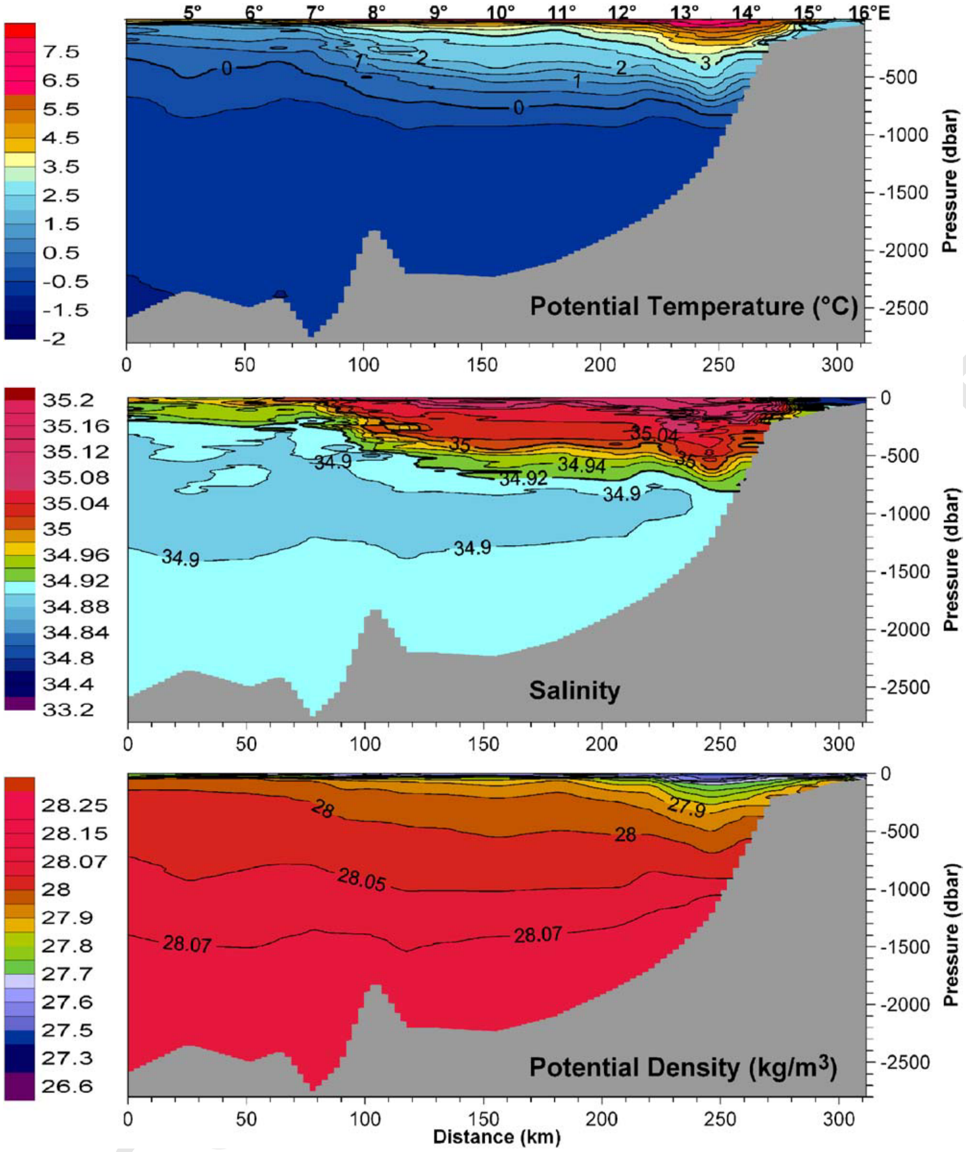

Fig. 4. Section ‘N’. Distribution of potential temperature, salinity, and potential density.

and that it is very strong between sections ‘Z’ and ‘EB’. This is confirmed by the horizontal current distribution (Fig. 5).

Table 2 presents only the heat carried by AW. Heat transport increases with latitude between sections ‘S’ and ‘Z’, even when AW transport decreases. Heat transport depends on water velocity and temperature, and in this case, differences can be explained by the non-homogenous horizontal distribution of the temperature field (Fig. 3).

4.2. VM-ADCP results

The current patterns obtained in sections with the VM-ADCP (Fig. 7) are similar to calculated baroclinic flows, although the measured values are higher. The highest velocities, with a maximal current speed of 43 cm s^{-1}, were observed above the continental slope within the core of the WSC. The second flow maximum is related to the Knipovich Ridge, where the maximum velocity measured was 29 cm s^{-1}. Thanks to the high spatial resolution of VM-ADCP measurements, the details of the structure of WSC are clearly visible (Fig. 8). There are alternating bands of northward and southward flows including strong northward flows associated with topographic features. The velocity structure is more complicated than that obtained from baroclinic calculations. VM-ADCP and geostrophic velocity vertical shear is similar, except in the upper layer, where ageostrophic signals are included.

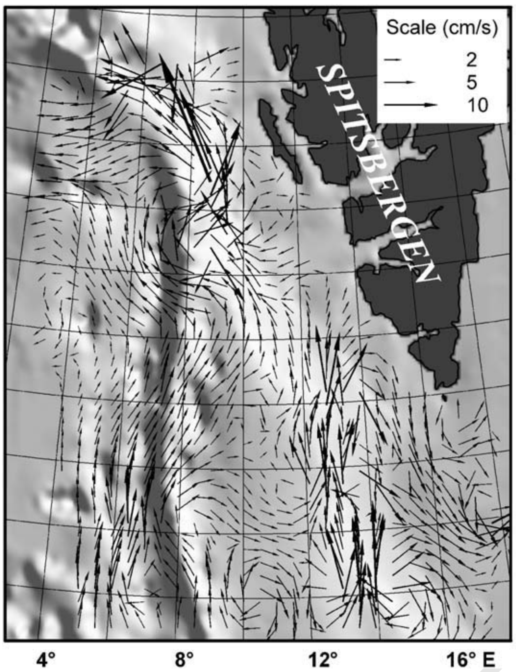

Fig. 5. Baroclinic currents at 100 dbar.

Fig. 9b presents velocities across section ‘N’ calculated from hydrographic and VM-ADCP data. ADCP-referenced barotropic velocities show about 5 cm s^{-1} to the north and 2 cm s^{-1} to the south. The current structure is fairly consistent with the LADCP measurements (Fig. 9c); there are only a few exceptions, especially to the west of the continental slope at 170–220 km. The VM-ADCP reference velocities were lower than those measured with LADCP. The best agreement in both current direction and speed was found above the Knipovich Ridge.

Table 3 contains the results of transport computed for sections ‘N’ and ‘K’. The net volume transports were 3–4 times higher than the calculated baroclinic ones. This reflects the importance of the barotropic component of the flows in the region of the WSC, which amounts to 7–8 Sv.

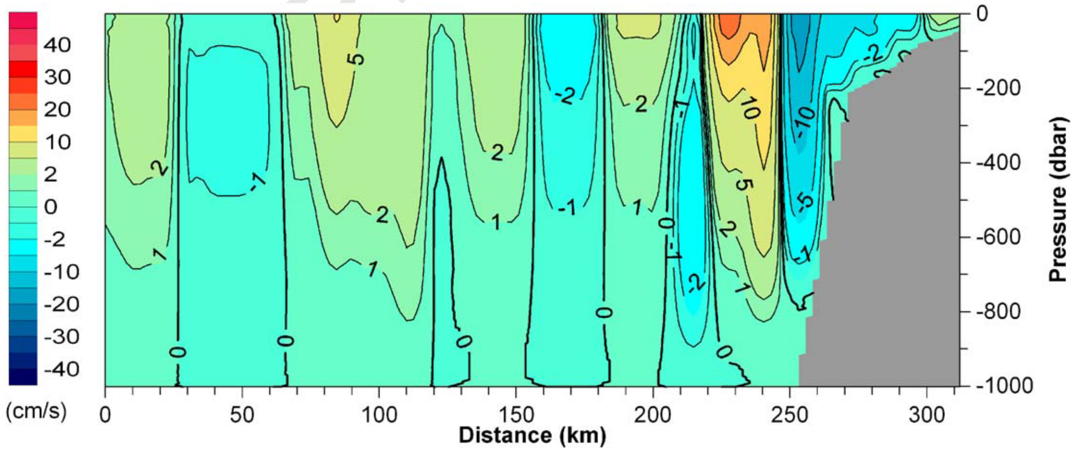

Fig. 6. Baroclinic currents in the upper 1000 m of the section ‘N’.

Table 2
Geostrophic volume and heat transport across sections K, N, S, Z, EB, Atlantic Water ($S > 34.92$, $\theta > 0\,^{\circ}$C) temperature and transports

Section	Volume transport (Sv)			AW temperature (°C)	AW volume transport (Sv)			AW heat transport (TW)
	Net	Northward	Southward		Net	Northward	Southward	
K	3.3	6.0	2.7	3.129	2.6	5.1	2.5	40.5
N	1.9	3.6	1.7	2.427	1.5	2.9	1.4	18.9
S	2.0	3.7	1.7	2.145	1.8	3.2	1.4	21.3
Z	1.6	2.1	0.6	2.210	1.6	1.9	0.3	23.4
EB	0.4	1.1	0.7	2.588	0.5	0.9	0.4	10.1

Reference level of no motion = 1000 dbar.

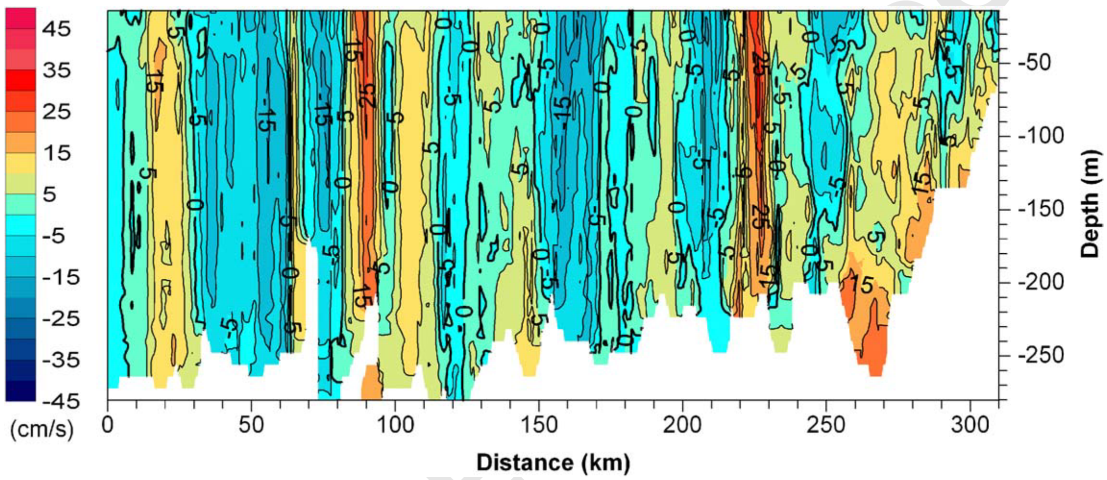

Fig. 7. VM-ADCP-measured currents in the upper 275 m of the section ‘N’.

4.3. LADCP results

Direct current measurements taken with the lowered ADCP permits profiling the entire water column during standard CTD casts. The vertical profile revealed that there is a zone with a near-homogeneous current between the bottom and a depth of 500 m, and layer of high-current shear above 500 m (Fig. 10). Other profiles also show that the flow has a strong barotropic component. In the near-bottom layer over the slope, the northward component of the current, measured in relation to the bottom (bottom tracked), is of the order of 5 cm s^{-1}. At some stations it is as high as 15 cm s^{-1}. In deepwater regions, a barotropic component occurs as well; the V-component in the near-bottom layer can reach 5 cm s^{-1}.

Fig. 9c presents LADCP-measured currents perpendicular to section ‘N’ (V-component). The general pattern of northward flow is similar to the patterns calculated using hydrographic data (Fig. 9a), although a pronounced barotropic constituent is visible in the current. This is the main reason that the volume and heat transports obtained for all sections were higher than the other estimates (Table 4).

There are considerable differences among total transport across several sections, especially between sections ‘N’ and ‘S’ or ‘Z’. This proves indirectly the high temporal variability of the WSC

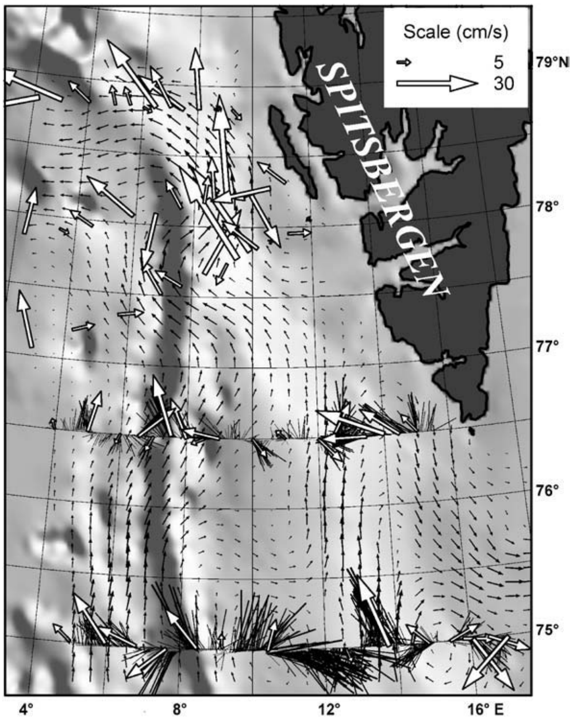

Fig. 8. Currents at 100 m measured by means of VM-ADCP (sticks) and LADCP (white arrows). The smoothed baroclinic currents are presented in the background.

dynamics. The measurements at section 'S' were conducted five days after those at section 'N', and, during this time southerly winds increased from 0 to 10 m s^{-1} (Table 1). These changes in weather conditions induced high barotropic flow; the bottom-tracked V-component of the current in the near-bottom layer reached 15 cm s^{-1} in the center of section 'Z'.

The mean velocity errors estimate using LDEO 7.0 software are, for most of the LADCP profiles, of the order of 2 cm s^{-1}, which is comparable with other results (Fischer et al., 2003). Error changes with depth; the bottom-tracked velocity has lower error than that measured near the surface (up to 5 cm s^{-1}). Differences between VM-ADCP and LADCP results are within the margins of error. Fischer and Visbeck (1993) discussed the quality of the LADCP data in detail.

The estimated volume transport errors take into account the bias related to the uncertainty of LADCP measurements and gridding procedures. In the case of the grid of section 'N', the mean velocity residual is -0.12 cm s^{-1} with a standard deviation of 2 cm s^{-1}. Other sources of uncertainties, such as horizontal measurements resolution that is too low or time lag between measurements, were not included. However, the horizontal resolution of sections was relatively high and was better than the existing current meter array (Fahrbach et al., 2001; Schauer et al., 2004) but is still lower than the Rossby radius of deformation.

5. Structure of the transports

There is good agreement between the VM-ADCP and LADCP measurements. Much larger differences exist between calculated baroclinic currents and those measured in situ. The largest differences appear over the shelf where the barotropic flow is the most intense.

However, both LADCP and baroclinic results show that AW transport had multi-path structures (Figs. 11 and 12). Analysis of section 'K' indicated that there were three streams of AW. The westernmost stream disappeared downstream. The distance between the branches over the slope and over the ridge decreased with latitude due to bottom topography convergences. In the case of baroclinic transports, the branch over the slope (Svalbard branch) almost disappeared in section 'EB'.

To compare transport across several sections, 150 km-long fractions of each section were chosen. Each fraction begun over the slope, east of the WSC core, contained a slope branch of the WSC and extended 150 km westward. Table 5 presents the transports and mean velocities calculated from LADCP data for three layers: surface to bottom, upper 1000 m, and from 1000 m to bottom. The current's structure varied both horizontally and vertically. In sections 'K' and 'N', most of the transport was concentrated in the upper 1000 m, in section 'S' it was divided between the upper and lower level. Section 'Z' was different; most of the transport was in the lower layer. The mean velocities here were higher in the lower layer than

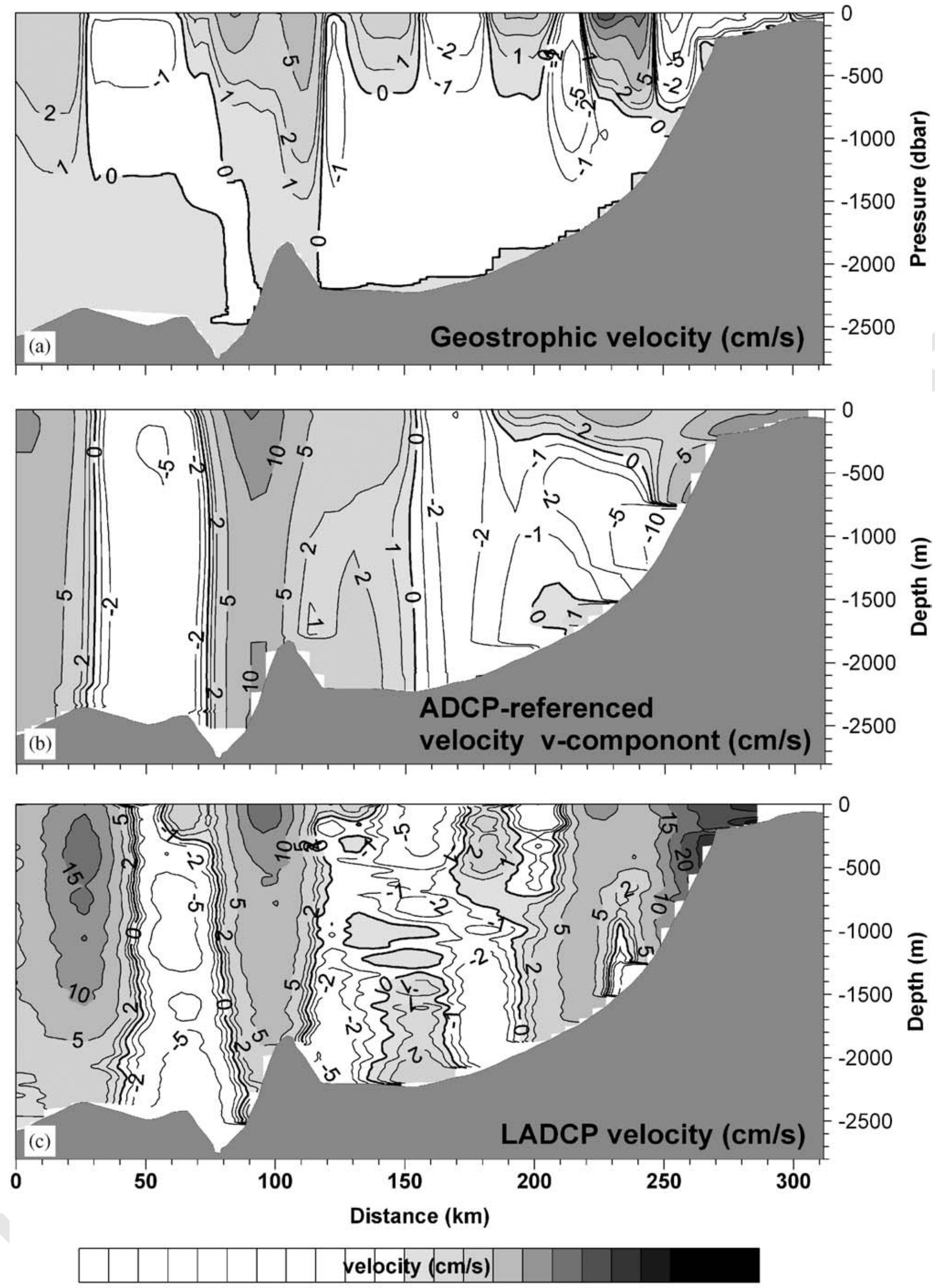

Fig. 9. Currents perpendicular to section 'N' calculated from (a) hydrological data (baroclinic method with bottom as no-motion layer); (b) mixed VM-ADCP and baroclinic results; (c) decided LADCP measurements.

Table 3
VM-ADCP-referenced geostrophic transports across sections K and N

Section	Volume transport (Sv)			AW volume transport (Sv)			AW heat transport (TW)
	Net	Northward	Southward	Net	Northward	Southward	
K	11.5±2.2	21.3	9.8	3.5	8.7	−5.1	52.4±10.0
N	9.0±2.0	17.6	8.6	3.3	4.9	−1.6	40.0±8.9

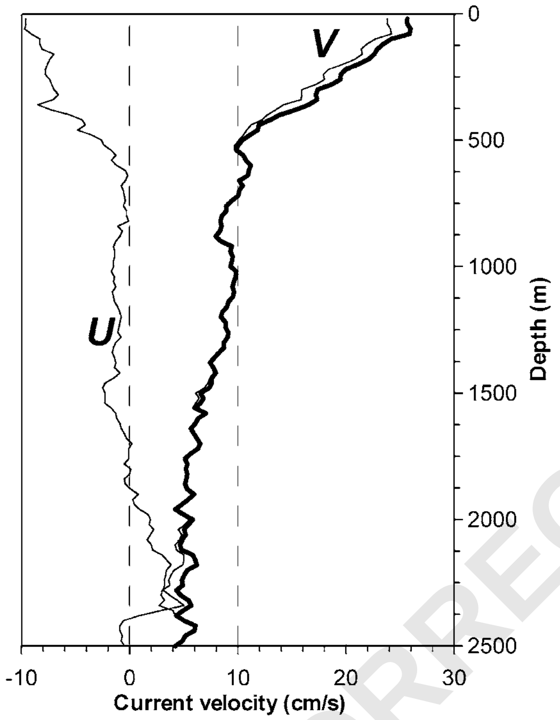

Fig. 10. Vertical LADCP profile at station N-5. Bold line indicates absolute velocity, thick lines mark the *U* and *V* components of the current profile.

in the upper one. In section ‘EB’ the ‘usual’ structure was noted again; higher velocities and transports were recorded in the surface layer. Although total transport across section ‘Z’ was much higher than across section ‘EB’, AW transport in cross-section ‘EB’ was larger (Table 6). This is a reasonable finding since the velocity in the upper layer of this section was higher than in section ‘Z’.

6. Discussion and concluding remarks

Vessel-based current measurements and all transport calculations are imprecise. VM-ADCP measures currents in the upper layer only and does not permit calculating transport throughout the whole water column. LADCP allows profiling throughout the entire water column, but has a relatively high margin of error.

Generally, transport calculations depend on station spacing and measurement accuracy. Additionally, the investigated processes are non-stationary, and sections treated as synoptic are affected by space–time sampling limitations. For hydrography-based calculations, the most important source of error is the reference velocity; 2.5 cm s^{-1} of barotropic current across a 200 km-long and 2000 m-deep section produces volume transport of 10 Sv. Reference levels are chosen arbitrarily and exclude the barotropic component of the flow. In the case of the WSC, the layer of no movement (LNM) did not exist (Cisewski et al., 2003), so it was reasonable to calculate the baroclinic flow using the bottom as LNM. Meanwhile, the baroclinic transports presented in this paper were calculated in reference to a 1000 dbar LNM to facilitate comparisons with other published data. A change of LNM from 1000 dbar to the bottom caused changes of up to 40% in baroclinic transport calculations presented in this paper. Theoretically, inverse modeling should eliminate uncertainties produced by the baroclinic method, but in the case of the WSC the barotropic flows are usually underestimated. Although moored current meters produce the best accuracy at a fixed point, total volume transport calcula-

Table 4
Cross-section transports calculated from LADCP data for entire sections

Section	Volume transport (Sv)			AW volume transport (Sv)			Area (km^2)	
	Net	Northward	Southward	Net	Northward	Southward	Total	AW
K	21.9±6.6	25.7	3.8	9.7±2.3	10.9	1.2	664.2	195.7
N	14.9±3.6	20.9	6.0	7.1±1.6	8.1	1	550.1	139.1
S	24.6±9.3	26.6	2.0	7.5±2.1	8.4	0.9	436.9	103.0
Z	28.6±7.7	32.6	3.1	4.5±1.4	5.4	0.9	438.6	75.5
EB	11.6±4.5	13.5	1.9	6.0±4.5	6.3	0.3	249.3	77.6

tions depend strongly on horizontal and vertical current meter array resolution.

The results presented here were obtained using various methods and substantial differences appeared. The highest values of both volume and heat transport were obtained by calculations based on direct LADCP observations, and the lowest were those based on baroclinic calculations. LADCP results regarding both volume and heat transport are also high in comparison with earlier geostrophic calculations (Rudels, 1987; Schlichtholz and Houssais, 1999). However, they are close to results obtained by Fahrbach et al. (2001) and Schauer et al. (2004), which were derived from data of moored instruments. There is also good agreement between the presented transport figures and findings published by Cisewski et al. (2003); for September 1997 they estimated northward volume transport at 11.5 Sv, and heat transport at 42 TW across the section along the 79°40′N parallel.

Good agreement with the VM-ADCP results and with other measurement–based transport calculations allows the authors to conclude that the results obtained with the LADCP provide the most representative values of quasi-synoptic currents and volume transports for this region of the WSC. The final values of transport across the sections 'K', 'N', 'S', 'Z', and 'EB' are shown in Table 7. However, even flows across the northernmost section do not represent the net volume and heat transported by Atlantic Water (AW) into the Arctic Ocean (AO), because of AW recirculation, which is not covered by the sections.

The results presented in this paper also indicate how important the barotropic component is in the case of the WSC. The similarity of the baroclinic calculations conducted by authors with other baroclinic estimates indicates that the barotropic component of the flow has usually been underestimated.

Even transports obtained using VM-ADCP and the mixed method, are lower than those calculated from direct LADCP measurements. Averaging between stations or ageostrophic flows might be responsible for this.

There are considerable differences in the estimated LADCP transport across different sections. The modification of the current due to wind conditions could be one of the reasons for this. The increase in the barotropic component of the flow in section 'Z' as compared with section 'N' was observed. The mean velocity of the lower layer at transect 'Z' is higher than the upper one (Table 5).

Information regarding the short-term variability of the WSC is insufficient. Fahrbach et al. (2001) reported that it exhibited a strong annual cycle and monthly fluctuation, but short-term variability was eliminated from the monthly means. Fahrbach (personal communication) observed high temporal variability in the northward volume transport across the 78°55′ section. The daily means of northward transport obtained from current meters in summer 2003 were from 10 to 30 Sv.

High current variability was reported by Orvik and Niiler (2002) for the eastern branch of the Norwegian Atlantic Current (NAC). The mean

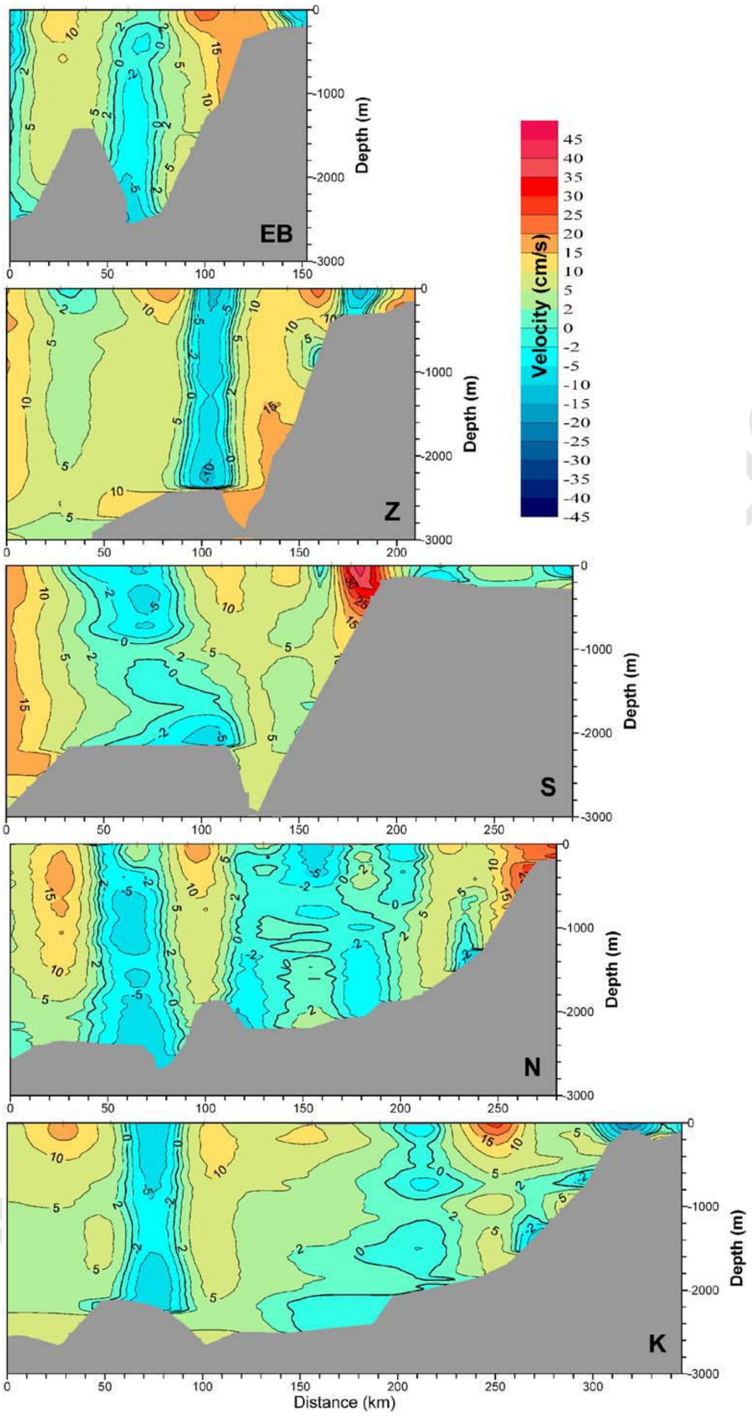

Fig. 11. LADCP measured current across sections 'EB','Z', 'S', 'N', and 'K'.

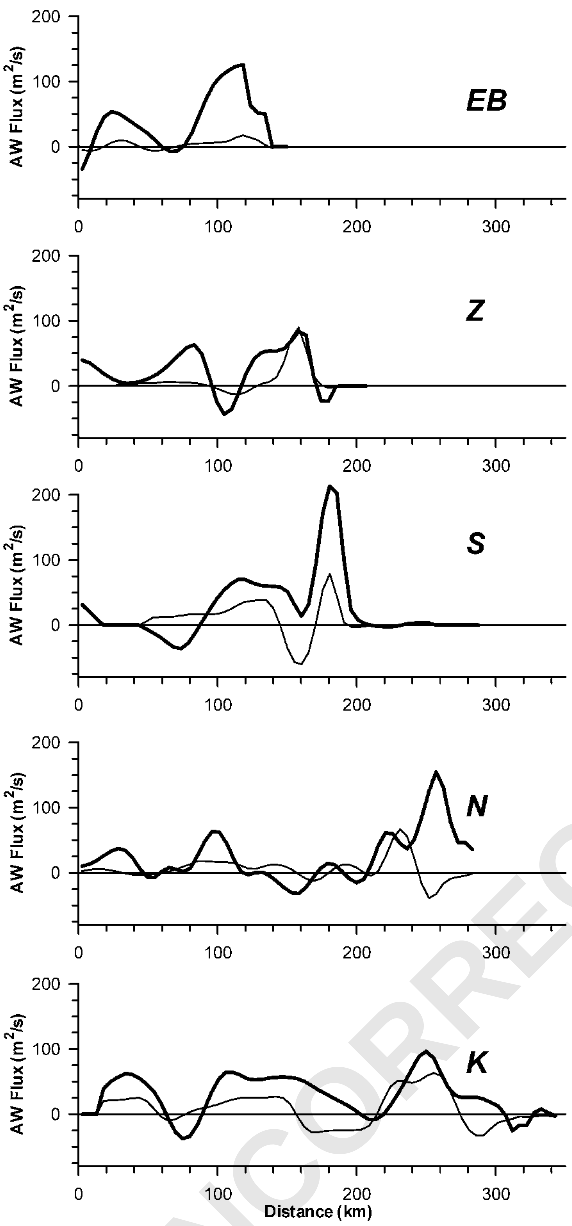

Fig. 12. Vertically integrated AW fluxes from LADCP (bold lines) and baroclinic calculations for sections 'EB','Z', 'S', 'N', and 'K'.

flow (4.2 Sv) across the Svinøy section varied within a 25 h-timeframe and ranged from −2.2 to 11.8 Sv. The WSC is the direct continuation of this topographically trapped branch of the NAC, thus similar variability in the WSC in the Fram Strait region can be expected. Ingvaldsen et al. (2004) also reported high temporal variability of AO inflow into the Barents Sea through the Barents Sea Opening (BSO).

The relation observed between volume transport and wind direction allows for speculation about possible mechanisms of current acceleration. The process has two stages. The first is wind-induced Ekman transport. Southern and south-eastern winds blowing along the Spitsbergen coast cause eastward flow towards the coast within the Ekman layer. This causes the inclination of the sea level perpendicular to the shelf break. Next, the tilt of the water forces geostrophic, barotropic flows parallel to the Spitsbergen coast. Calculation using geostrophic balance formula indicates that at this latitude 10 cm of sea level difference per 100 km causes 7 cm s^{-1} of barotropic flow. Wind blowing from the N–NW direction lowers the water level along Spitsbergen and reverses the current direction. In reality, the mechanism is much more complicated; inhomogeneous atmospheric pressure and wind field can produce Kelvin waves, also bottom friction is important. Analysis of these processes is beyond the scope of the current paper.

Investigations performed aboard the R.V. *Oceania* in 2004 indicate that the time lag between changing wind direction and the changing direction of the net volume transport is of the order of 1 day. Measurements repeated three times across section 'EB' show a reversal of the net volume transport within 3 days.

Ingvaldsen et al. (2004) also point out the importance of local wind conditions for AW inflow. The mechanism of inducing barotropic flows across the BSO proposed by them is similar. The data from current meters that were analyzed were filtered to remove fluctuations within periods of less than 2 weeks, but higher frequency variability is also described; complete current reversal was observed on a time scale of 1–2 days.

Another feature of the measured transport that requires discussion is the difference between AW transports across sections 'Z' and 'EB'. Although the differences are within the margin of error, this might be explained by mesoscale activity. Eddies and meanders play a significant role in shaping

Table 5
Cross-section transports calculated from LADCP results for 150-km-long sections

Section	Area (km^2)	Volume transport (Sv)					Mean velocity ($cm\,s^{-1}$)		
		Surface to bottom			Surface to 1000 m	1000 m to bottom	Surface to bottom	Surface to 1000 m	1000 m to bottom
		Net	Northward	Southward					
K	284.7	7.6	8.4	0.8	6.0	1.6	2.6	4.1	1.1
N	242.4	5.7	7.7	2.0	5.0	0.7	2.4	3.7	0.7
S	319.6	12.7	14.6	1.9	8.3	4.4	4.0	5.5	2.6
Z	363.8	22.5	25.2	2.7	7.9	14.6	6.2	5.4	6.7
EB	249.3	11.6	13.5	1.9	8.6	3.0	4.6	6.6	2.6

Table 6
Cross-section transport of AW from LADCP results for 150-km-long sections

Section	AW area (km^2)	AW volume transport (Sv)			AW mean properties			AW heat transport (TW)
		Net	Northward	Southward	Velocity ($cm\,s^{-1}$)	Temperature (°C)	Salinity	
K	110.5	5.2	5.4	0.2	4.7	3.1	35.04	85.3
N	97.3	5.8	7.8	2	4.5	2.6	35.02	60.4
S	92.0	6.4	7.3	0.9	7.0	1.9	34.99	81.8
Z	65.5	4.1	4.7	0.6	6.3	2.2	34.99	43.4
EB	77.6	6.0	6.3	0.3	7.7	2.5	35.00	75.4

Table 7
Transports calculated from LADCP data for entire sections

Section	Net transports entire sections		AW transports $S>34.92$, $\theta>0\,°C$		AW transports $S>34.90$, $\theta>3\,°C$	
	Volume (Sv)	Heat (TW)	Volume (Sv)	Heat (TW)	Volume (Sv)	Heat (TW)
K	21.9 ± 6.6	112.4 ± 33.7	9.7 ± 2.3	133.4 ± 32.0	5.5 ± 1.7	29.4 ± 8.8
N	14.9 ± 3.6	78.0 ± 18.7	7.1 ± 1.6	84.2 ± 18.5	2.8 ± 0.7	18.1 ± 4.3
S	24.6 ± 9.3	61.7 ± 23.4	7.5 ± 2.1	96.6 ± 27.0	3.5 ± 1.0	18.7 ± 5.2
Z	29.5 ± 7.7	-16.3 ± 4.2	4.5 ± 1.4	42.1 ± 12.6	1.2 ± 0.4	7.3 ± 2.2
EB	11.6 ± 4.5	70.6 ± 27.5	6.0 ± 2.3	75.4 ± 29.4	2.8 ± 1.1	15.0 ± 5.8

Two AW parameterizations are used.

WSC transport (Gascard et al., 1995; Cisewski et al., 2003). The horizontal temperature distribution (Fig. 3) and the higher AW temperature at section 'EB' (Table 6) suggests that AW transport resulting from mesoscale activity occurred during the current experiment.

Direct LADCP measurements confirm the multi-path structure of the WSC in the region of western Spitsbergen. However, the WSC also has a complicated structure in the southern part. In addition to the main stream of AW that continues along the Barents Sea shelf break, a second colder and fresher branch of the AW fed by the Arctic Front jet streams flows over the Knipovich Ridge. The hydrographic and LADCP results show that these two streams of AW converge in the region of central Spitsbergen; the shortest distance between both branches, due to the bottom topography is at 77°N. Further to the north both streams diverge. The western one recirculates, the eastern splits into the three branches described earlier.

The western branch structure is similar to that described by Poulain et al. (1996) and Orvik et al. (2001) for the southern Norwegian Sea. They describe the inflow of AW as a bifurcated system with a warmer stream trapped by the shelf break in the east and the colder frontal jets of the Polar Front (in this paper the Arctic Front (AF)) in the west. Orvik and Niiler (2002) suggest that this system continues towards the Fram Strait. Van Aken et al. (1995) describe the frontal jets of AF carrying AW northward. This branch of AW does not reach the AO. Part of AW flowing along the AF crosses the front over the Mohns Ridge (Piechura and Walczowski 1995), the rest recirculates westward in the Fram Strait region.

LADCP measurements provide valuable information about flow structure that can be helpful in the analysis of current meter data. Understanding the structure of the flow field can help to interpolate data and to complement it. More generally, it can be concluded that despite significant progress, determining volume and heat balance in the AO is far from precise. The only way of producing satisfactory results is to link results from all available sources such as modeling, moorings, synoptic observations, satellite altimetry, etc. The high spatial and temporal variability of the investigated fields also means that determining the interannual variability of water mass properties and transports based on synoptic sections performed a few times per year should be treated with caution.

Acknowledgements

We are grateful to Ilona Goszczko, Roman Obuchowski, Krzysztof Rosinski and all R.V. *Oceania* crew, who participated in the work at the sea. Special acknowledge to Eberhard Fahrbach and Agnieszka Beszczynska for information and discussion about Fram Strait flows. We thank editor and anonymous reviewers for their very helpful and constructive comments.

This research has been supported by grant from the European Union's Fifth Framework Program project ASOF-N (Arctic-Subarctic Ocean Flux Array for European Climate: North), contract number EVK2-CT-200200139.

References

Aagaard, K., Carmack, E.C., 1989. The role of sea ice and other fresh water in the Arctic circulation. Journal of Geophysical Research 94 (C14), 14 485–14 498.

Aagaard, K., Darnall, C., Greisman, P., 1973. Year-long current measurements in the Greenland-Spitsbergen passage. Deep-Sea Research 20, 743–746.

Aagaard, K., Foldvik, A., Hillman, S.R., 1987. The West Spitsbergen Current: disposition and water mass transformation. Journal of Geophysical Research 92, 3778–3784.

Bourke, R.H., Wiegel, A.M., Paquette, R.G., 1988. The westward turning branch of the West Spitsbergen Current. Journal of Geophysical Research 93, 14 065–14 077.

Bretherton, F.P., Davis, R.E., Fandry, C.B., 1976. A technique for objective analysis and design of oceanographic experiments applied to MODE-73. Deep-Sea Research 23, 559–582.

Cisewski, B., Budéus, G., Krause, G., 2003. Absolute transport estimates of total and individual water masses in the northern Greenland Sea derived from hydrographic and acoustic Doppler current profiler measurements. Journal of Geophysical Research 108 (C9).

Cokelet, E.D., Schall, M.L., Dougherty, D.M., 1996. ADCP-referenced geostrophic circulation in the Bering Sea Basin. Journal of Physical Oceanography 26, 1113–1128.

Dickson, R.R., Osborn, T.J., Hurrell, J.W., Meincke, J., Blindheim, J., Adlandsvik, B., Vinje, T., Alekseev, G., Maslowski, W., 2000. The Arctic Ocean response to the North Atlantic oscillation. Journal of Climate 13 (15), 2671–2696.

Emery, W.J., Thomson, R.E., 2001. Data Analysis Methods in Physical Oceanography. Elsevier Science B.V., Amsterdam.

Fahrbach, E., Meincke, J., Østerhus, S., Rohardt, G., Schauer, U., Tverberg, V., Verduin, J., 2001. Direct measurements of volume transports through Fram Strait. Polar Research 20 (2), 217–224.

Fischer, J., Visbeck, M., 1993. Deep velocity profiling with self-containing ADCPs. Journal of Atmospheric and Oceanic Technology 10, 764–773.

Fischer, J., Brandt, P., Denger, M., Müller, M., Symonds, D., 2003. Surveying the upper ocean with the ocean surveyor: a new phased array doppler current profiler. Journal of Atmospheric and Oceanic Technology 20, 742–751.

Friedrich, H., Houssais, M.N., Quadfasel, D., Rudels, B., 1995. On Fram Strait water masses. Extended Abstract, Nordic Seas Symposium, Hamburg, pp. 69–72

Gascard, J.C., Richez, C., Roaualt, C., 1995. New insights on large-scale oceanography in Fram Strait: the West Spitsbergen Current. In: Smith Jr., W.O., Grebmeier, J.M. (Eds.), Arctic Oceanography, Marginal Ice Zones and Continental Shelves. AGU 49, Washington DC, pp. 131–182.

Hansen, B., Østerhus, S., 2000. North Atlantic-Nordic Seas exchanges. Progress in Oceanography 45, 109–208.

Hanzlick, D.J., 1983. The West Spitsbergen Current: transport, forcing and variability. Ph.D. Thesis, University of Washington, 127pp.

Hopkins, T., 1991. The GIN sea—A synthesis of its physical oceanography and literature review 1972–1985. Earth-Science Review 30 (3–4), 175–318.

Ingvaldsen, R.B., Asplin, L., Loeng, H., 2004. Velocity field of the western entrance to the Barents Sea. Journal of Geophysical Research 109, C03021.

Johannessen, O.M., 1986. Brief Overview of the Physical Oceanography. The Nordic Seas. Springer, Berlin, New York, pp. 103–127, Chapter 4.

Karcher, M.J., Gerdes, R., Kauker, F., Koberle, C., 2003. Arctic warming: evolution and spreading of the 1990s warm event in the Nordic seas and the Arctic Ocean. Journal of Geophysical Research 108 (C2).

Kowalik, Z., 1994. Modeling of topographically amplified diurnal tides in the Nordic Seas. Journal of Physical Oceanography 24, 1717–1731.

Kowalik, Z., Proshutinsky, Y.A., 1995. Topographic enhancement of tidal motion in the western Barents Sea. Journal of Geophysical Research 100 (C2), 2613–2637.

Manley, T.O., 1995. Branching of Atlantic Water within the Greenland-Spitsbergen Passage: an estimate of recirculation. Journal of Geophysical Research 100 (C10), 20 627–20 634.

Maslowski, W., Marble, D., Walczowski, W., Schauer, U., Clement, J.L., Semtner, A.J., 2004. On climatological mass, heat, and salt transports through the Barents Sea and Fram Strait from a pan-Arctic coupled ice-ocean model simulation. Journal of Geophysical Research 109 (C3).

Meinen, C.S., Watts, D.R., Clarke, R.A., 2000. Absolutely referenced geostrophic velocity and transport on a section across the North Atlantic Current. Deep-Sea Research I 47, 309–322.

Orvik, K.A., Niiler, P., 2002. Major pathways of Atlantic water in the northern North Atlantic and Nordic Seas toward Arctic. Geophysical Research Letters 29 (19), 1896–1899.

Orvik, K.A., Skagseth, Ø., 2003. Monitoring the Norwegian Atlantic slope current using a single moored current meter. Continental Shelf Research 23, 159–176.

Orvik, K.A., Skagseth, Ø., Mork, M., 2001. Atlantic inflow to the Nordic Seas: current structure and volume fluxes from moored current meters, VM-ADCP and SeaSoar-CTD observations, 1995–1999. Deep-Sea Research I 48, 937–957.

Osinski, R., Wieczorek, P., Beszczynska-Moller, A., Goszczko, I., 2003. ADCP-referenced geostrophic velocity and transport in the West Spitsbergen Current. Oceanologia 45 (3), 425–435.

Perkin, R.G., Lewis, E.L., 1984. Mixing in the West Spitsbergen Current. Journal of Physical Oceanography 14, 1315–1325.

Piechura, J., Walczowski, W., 1995. The Arctic Front: structure and dynamics. Oceanologia 37 (1), 47–73.

Piechura, J., Beszczynska-Moller, A., Osinski, R., 2001. Volume, heat and salt transport by the West Spitsbergen Current. Polar Research 20 (2), 233–240.

Piechura, J., Osiński, R., Petelski, T., Woźniak, S.B., 2002. Heat and salt fluxes in the West Spitsbergen Current in summer time. Oceanologia 44 (3), 307–321.

Poulain, P.M., Warn-Varnas, A., Niiler, P.P., 1996. Near-surface circulation of the Nordic seas as measured by Lagrangian drifters. Journal of Geophysical Research 101 (C8), 18 237–18 258.

Quadfasel, D., Gascard, J.C., Koltermann, K.P., 1987. Large-scale oceanography in Fram Strait during the 1984 Marginal Ice Zone experiment. Journal of Geophysical Research 92, 6719–6728.

Rudels, B., 1987. On the mass balance of the Polar Ocean, with special emphasis on the Fram Strait. Norwegian Polar Institute, Skr.188, 53pp.

Rudels, B., Meyer, R., Fahrbach, E., Ivanov, V.V., Østerhus, S., Quadfasel, D., Schauer, U., Tverberg, V., Woodgate, R.A., 2000. Water mass distribution in Fram Strait and over the Yermak Plateau in summer 1997. Annales Geophisicae 18, 687–705.

Saloranta, T.M., Haugan, P.M., 2001. Interannual variability of the hydrography of Atlantic water northwest of Svalbard. Journal of Geophysical Research 106 (C7), 13 931–13 943.

Schauer, U., Loeng, H., Rudels, B., Ozhigin, V., Dieck, W., 2002. Atlantic Water flow throught the Barents and Kara Sea. Deep-Sea Research I 49, 2281–2296.

Schauer, U., Fahrbach, E., Osterhus, S., Rohardt, G., 2004. Arctic warming through the Fram Strait: oceanic heat transport from 3 years of measurements. Journal of Geophysical Research 109, C06026.

Schlichtholz, P., Houssais, M.N., 1999. An inverse modeling study in Fram Strait. Part I, Part II: dynamics and circulation. Deep-Sea Research II 46, 1083–1168.

Simonsen, K., Haugan, P.M., 1996. Heat budgets of the Arctic Mediterranean and sea surface heat flux parameterizations for the Nordic Seas. Journal of Geophysical Research 101 (C3), 6553–6576.

Swift, J.H., 1986. The Arctic waters. In: Hurdle, B.G. (Ed.), The Nordic Seas. Springer, New York, pp. 129–153.

Swift, J.H., Aagaard, K., 1981. Seasonal transitions and water mass formation in the Iceland and Greenland Sea. Deep-Sea Research 28, 1107–1129.

van Aken, H.M., Budeus, K., Hahnel, M., 1995. The Anatomy of the Arctic Frontal Zone in the Greenland Sea. Journal of Geophysical Research 100 (C8), 15 999–16 9014.

Zhang, J., Rothrock, D.A., Steele, M., 1998. Warming of the Arctic Ocean by a strengthened Atlantic inflow: model results. Geophysical Research Letters 25, 1745–1748.